R. & M. No. 3214

R. & M. No. 3214

MINISTRY OF AVIATION

AERONAUTICAL RESEARCH COUNCIL
REPORTS AND MEMORANDA

Theoretical Subsonic Derivatives for an Oscillating M-Wing

By H. C. GARNER, M.A., A.F.R.Ae.S.
and W. E. A. ACUM, A.R.C.S., B.Sc.
OF THE AERODYNAMICS DIVISION, N.P.L.

LONDON: HER MAJESTY'S STATIONERY OFFICE
1961
PRICE: 11*s.* 0*d.* NET

Theoretical Subsonic Derivatives for an Oscillating M-Wing

By H. C. Garner, M.A., A.F.R.Ae.S.
and W. E. A. Acum, A.R.C.S., B.Sc.
of the Aerodynamics Division, N.P.L.

*Reports and Memoranda No. 3214**
January, 1959

Summary. The report describes a theoretical investigation in support of measurements being made on an oscillating half-wing model of the plan-form shown in Fig. 1 in the National Physical Laboratory 25 in. by 20 in. Wind Tunnel fitted with slotted liners. Little is known about the steady or unsteady characteristics of M-wings. Results are obtained by low-frequency theory at Mach numbers 0 and 0·8 and by general theory for frequency parameters 0·3 and 0·6 (based on mean chord) at the Mach number 0·8. The calculations cater for rigid pitching about an arbitrary axis and rigid bending about the wing root, the latter mode being used experimentally to estimate forces on a complete rolling M-wing.

The sharp kinks located at the root and mid-semi-span of the leading and trailing edges subject the theories to a severe test. The calculated steady characteristics reveal a very slow rearward trend in aerodynamic centre as Mach number increases and large discrepancies in the local aerodynamic centre over the outer panel of the M-wing. The oscillatory characteristics are summarized in tables of the calculated pitching and bending derivatives, the former being given numerically for the three pitching axes for which provision is made in the experiments. The figures show how the derivatives vary with axis position, frequency parameter and Mach number.

As compared with conventional delta or arrowhead plan-forms, the M-wing has a high minimum pitching damping at low speeds, which occurs for a pitching axis close to the aerodynamic centre. Although a change in frequency parameter from 0 to 0·6 reduces the damping derivative about rearward axes by roughly 30 per cent, the pitching oscillation shows no likelihood of becoming undamped. The error in the calculated values of the damping about all practical pitching axes may be as much as 15 per cent of its minimum value; only half this inaccuracy is incurred in the other derivatives. Nevertheless, exceedingly laborious calculations would probably be needed to establish their values to two places of decimals. The comparison between calculated and measured values of the pitching derivatives is good for the in-phase lift and moment and somewhat less satisfactory for the damping derivatives. The significance of the differences is doubtful, as slotted-wall interference effects in unsteady flow are unknown and there is reason to suppose that they may be large.

The symmetrical rigid-bending mode is highly damped for the range of frequency parameter. Some calculations with an antisymmetrical rolling mode have been made in order to estimate the corrections which must be applied to the experiments. It is shown that a factor of about 0·89 is necessary to convert the rigid-bending damping of the half-wing model to the rolling damping of the complete M-wing.

1. *Introduction.* The research programme of the N.P.L. includes the measurement of oscillatory aerodynamic derivatives in the speed range $0{\cdot}6 \leqslant M \leqslant 1{\cdot}4$ on a half-wing model having the plan-form shown in Fig. 1. The present report describes some theoretical calculations carried out

* Previously issued as A.R.C. 20,649.

for comparison with the derivatives measured in the subsonic range. The plan-form is of the so-called 'M-wing' type and has the special features of a kink at half-span, the inner panel having a quarter-chord sweep-forward of 55 deg and the outer panel a trailing-edge sweep-back of 55 deg and a leading edge of parabolic shape with its vertex at the pointed tip.

Although lifting-surface theories exist which have coped successfully with wings of more conventional plan-form, the M-wing must be expected to provide a severe test. Multhopp's theory[1,2] was used for steady flow and low-frequency oscillations at $M = 0$ and $M = 0{\cdot}8$, since it has appeared to be the most accurate; being almost completely mechanized, it can be applied rapidly. Although the experiments at $M = 0{\cdot}8$ have been made at one frequency parameter of about $\bar{\nu} = 0{\cdot}055$, the theoretical work at this Mach number covers the full practical range of frequency; for the higher values $\bar{\nu} = 0{\cdot}3$ and $0{\cdot}6$, the theory of Ref. 3 was applied, since this is also largely mechanized. In both these theories the collocation points lie at sections $y = s \sin [\pi n/(m+1)]$ where m is an odd integer and $n = 0, 1, \ldots, \frac{1}{2}(m-1)$. If $(m+1)$ is a multiple of 6, one of these sections, $y = \frac{1}{2}s$, contains the kink, which may then be treated by the procedure suggested in Ref. 1. Accordingly $m = 11$ was chosen for most of the calculations although a few low-frequency solutions with $m = 23$ were also obtained as a check on accuracy. The collocation points in a solution with $m = 11$ and two chordwise terms are shown in Fig. 1.

The modes for which experiments are being performed are firstly rigid pitching about three axes and secondly rigid bending of the half-model about a streamwise axis near its centre-line, the latter being intended to give some idea of the forces on the rigid rolling wing. The calculations have therefore been carried out for rigid pitching about an arbitrary axis, for symmetrical oscillations of the complete wing hinged along its centre section but otherwise rigid, and for steady rolling of the complete wing. Comparison of the last two calculations should give some idea of the corrections which must be applied to the experiments with bending mode in order to obtain the damping derivatives for rigid rolling oscillations.

2. *Calculations for Low Frequency.* Slow pitching and plunging oscillations of the M-wing were considered first by Multhopp's theory[1,2]. The logarithmic singularity in the spanwise integral for the downwash was treated by means of Ref. 4. In fact, the procedure in Appendix II of Ref. 2 was followed in the calculations with $N = 2$ chordwise terms.

The choice of the number of spanwise stations was dictated by the plan-form; by choosing m to be 11 and 23, the stations $\eta_n = \sin [n\pi/(m+1)]$ included $\eta = 0$ and $\eta = \frac{1}{2}$ where the kinks occur. The usual 'interpolated wing' was used, so that the local leading edge and chord at a kink station $\eta = \eta_n$ are replaced by

$$\left.\begin{aligned} x_{nl} &= \tfrac{1}{12}x_{n-1,l} + \tfrac{5}{6}(x_l)_{\text{kink}} + \tfrac{1}{12}x_{n+1,l} \\ c_n &= \tfrac{1}{12}c_{n-1} + \tfrac{5}{6}(c)_{\text{kink}} + \tfrac{1}{12}c_{n+1} \end{aligned}\right\}, \tag{1}$$

as indicated by the dotted curves in Fig. 1.

The theoretical calculations with $m(N) = 11(2)$ and $23(2)$ were made for both $M = 0$ and $M = 0{\cdot}8$. In addition, for $M = 0{\cdot}8$ only, a solution with $m(N) = 11(3)$ was obtained. The introduction of a third chordwise term involves a load distribution

$$l = \exp\left\{\frac{i\omega x M^2}{U(1-M^2)}\right\}\frac{8s}{\pi c}\left[\bar{\gamma}\cot\tfrac{1}{2}\phi + 4\bar{\mu}(\cot\tfrac{1}{2}\phi - 2\sin\phi) + \bar{\kappa}(\cot\tfrac{1}{2}\phi - 2\sin\phi - 2\sin 2\phi)\right], \tag{2}$$

where

$$x = x_l(\eta) + c(\eta)\,\tfrac{1}{2}(1-\cos\phi) \tag{3}$$

and $\bar{\gamma}$, $\bar{\mu}$ and $\bar{\kappa}$ depend on η. The consequent boundary condition is

$$-\frac{w}{U}\exp\left\{-\frac{i\omega x_\nu M^2}{U(1-M^2)}\right\} = b_{\nu\nu}[(\bar{i}_{\nu\nu}-\sigma_\nu\bar{\bar{i}}_{\nu\nu})\bar{\gamma}_\nu + (\bar{j}_{\nu\nu}-\sigma_\nu\bar{\bar{j}}_{\nu\nu})\bar{\mu}_\nu + (\bar{k}_{\nu\nu}-\sigma_\nu\bar{\bar{k}}_{\nu\nu})\bar{\kappa}_\nu]$$
$$-\sum_{-\frac{1}{2}(m-1)}^{\frac{1}{2}(m-1)}{}' b_{\nu n}[(i_{\nu n}-\sigma_n ii_{\nu n})\bar{\gamma}_n + (j_{\nu n}-\sigma_n jj_{\nu n})\bar{\mu}_n + (k_{\nu n}-\sigma_n kk_{\nu n})\bar{\kappa}_n], \tag{4}$$

where σ_n denotes the imaginary quantity $i\omega c_n/[U(1-M^2)]$. Equation (4) is satisfied at each combination of the m spanwise stations $\eta_\nu = \sin[\nu\pi/(m+1)]$ and the three chordwise stations $x_\nu = x_{\nu l} + \frac{1}{2}c_\nu(1-\cos\phi)$, where $\phi = 2\pi/7$, $4\pi/7$ and $6\pi/7$. The spanwise symmetry makes it unnecessary to consider negative ν, so that the resulting $\frac{3}{2}(m+1)$ complex equations with $\bar{\gamma}_{-n} = \bar{\gamma}_n$, $\bar{\mu}_{-n} = \bar{\mu}_n$ and $\bar{\kappa}_{-n} = \bar{\kappa}_n$ determine the complex unknowns $\bar{\gamma}_n$, $\bar{\mu}_n$ and $\bar{\kappa}_n$ for $n = 0, 1, \ldots \frac{1}{2}(m-1)$.

The influence functions i, ii, j, jj in Equation (4) are defined in Section 4 of Ref. 2; the two additional ones are given similarly by

$$\left.\begin{aligned} k(X,\,Y) &= \frac{1}{\pi}\int_0^\pi \frac{(2X-1+\cos\phi)(\cos 2\phi+\cos 3\phi)}{\{(2X-1+\cos\phi)^2+4Y^2\}^{1/2}}\,d\phi \\ kk(X,\,Y) &= \int_{-\infty}^{X} k(X_0,\,Y)\,dX_0 \end{aligned}\right\}, \tag{5}$$

where X and Y take values

$$\left.\begin{aligned} X_{\nu n} &= (x_\nu - x_{nl})/c_n \\ Y_{\nu n} &= (1-M^2)^{1/2}s(\eta_\nu-\eta_n)/c_n \end{aligned}\right\}. \tag{6}$$

There is a simple relationship

$$k = 2i - \tfrac{1}{4}j - 2jj\,, \tag{7}$$

but the corresponding expression for kk is more complicated. All the influence functions were evaluated by a mechanized programme for the DEUCE in the Mathematics Division, N.P.L.

It is necessary to distinguish between the method of Ref. 2 described above and the limiting form of Ref. 3 as the frequency parameter tends to zero. In place of Equation (2) the load distribution in Ref. 3 is

$$l = \exp\left\{-\frac{i\omega x}{U}\right\}\frac{8s}{\pi c}[\gamma\cot\tfrac{1}{2}\phi + 4\mu(\cot\tfrac{1}{2}\phi - 2\sin\phi)]\,. \tag{8}$$

Furthermore, the boundary condition (4) is multiplied by the factor

$$\exp\left\{\frac{i\omega x_\nu}{U}+\frac{i\omega x_\nu M^2}{U(1-M^2)}\right\} = 1 + \frac{i\omega x_\nu}{U(1-M^2)} + 0(\omega^2) \tag{9}$$

to give an equation

$$-\frac{w}{U}\exp\left\{\frac{i\omega x_\nu}{U}\right\} = b_{\nu\nu}[\bar{I}_{\nu\nu}\gamma_\nu + \bar{J}_{\nu\nu}\mu_\nu] - \sum_{-\frac{1}{2}(m-1)}^{\frac{1}{2}(m-1)}{}' b_{\nu n}[I_{\nu n}\gamma_n + J_{\nu n}\mu_n]\,. \tag{10}$$

With the aid of Equation (3), the load distribution (8) may be rewritten as

$$l = \exp\left\{\frac{i\omega x M^2}{U(1-M^2)}\right\}\frac{8s}{\pi c}\left[\gamma F_\gamma + \mu F_\mu\right], \tag{11}$$

where

$$F_\gamma = \cot\tfrac{1}{2}\phi\left\{1 - \frac{i\omega(x_l+\frac{1}{4}c)}{U(1-M^2)}\right\} + (\cot\tfrac{1}{2}\phi - 2\sin\phi)\left\{\frac{\frac{1}{4}i\omega c}{U(1-M^2)}\right\} \tag{12}$$

and

$$F_\mu = \cot\tfrac{1}{2}\phi\left\{\frac{\frac{1}{4}i\omega c}{U(1-M^2)}\right\} + (\cot\tfrac{1}{2}\phi - 2\sin\phi)\left\{1 - \frac{i\omega(x_l+\frac{1}{2}c)}{U(1-M^2)}\right\}$$
$$+ (\cot\tfrac{1}{2}\phi - 2\sin\phi - 2\sin 2\phi)\left\{\frac{\frac{1}{4}i\omega c}{U(1-M^2)}\right\}. \tag{13}$$

When the load distribution (11) replaces (2), it follows from Equation (12) that the complex influence function $(i_{\nu n} - \sigma_n ii_{\nu n})$ in Equation (4) is replaced by

$$i_{\nu n}\left\{1 - \frac{i\omega(x_{nl}+\frac{1}{4}c_n)}{U(1-M^2)}\right\} + \tfrac{1}{4}j_{\nu n}\left\{\frac{\frac{1}{4}i\omega c_n}{U(1-M^2)}\right\} - ii_{\nu n}\left\{\frac{i\omega c_n}{U(1-M^2)}\right\}.$$

With the factor (9), the corresponding influence function in Equation (10) is

$$I_{\nu n} = i_{\nu n} - \frac{i\omega}{U(1-M^2)}\left[(x_{nl}+\tfrac{1}{4}c_n - x_\nu)i_{\nu n} - \tfrac{1}{16}c_n j_{\nu n} + c_n ii_{\nu n}\right]$$
$$= i_{\nu n} - \sigma_n\left[(\tfrac{1}{4} - X_{\nu n})i_{\nu n} - \tfrac{1}{16}j_{\nu n} + ii_{\nu n}\right]. \tag{14}$$

Similarly, when the chordwise loading (13) is used instead of $(\cot\frac{1}{2}\phi - 2\sin\phi)$, there are extra terms in the influence function, so that $(j_{\nu n} - \sigma_n jj_{\nu n})$ in Equation (4) is replaced by

$$4i_{\nu n}\left\{\frac{\frac{1}{4}i\omega c_n}{U(1-M^2)}\right\} + j_{\nu n}\left\{1 - \frac{i\omega(x_{nl}+\frac{1}{2}c_n)}{U(1-M^2)}\right\} + 4k_{\nu n}\left\{\frac{\frac{1}{4}i\omega c_n}{U(1-M^2)}\right\} - jj_{\nu n}\left\{\frac{i\omega c_n}{U(1-M^2)}\right\}$$
$$= j_{\nu n}\left\{1 - \frac{i\omega(x_{nl}+\frac{1}{2}c_n)}{U(1-M^2)}\right\} + \frac{i\omega c_n}{U(1-M^2)}\left[3i_{\nu n} - \tfrac{1}{4}j_{\nu n} - 3jj_{\nu n}\right]$$

by Equation (7). Hence the factor (9) gives

$$J_{\nu n} = j_{\nu n} - \sigma_n\left[-3i_{\nu n} + (\tfrac{3}{4} - X_{\nu n})j_{\nu n} + 3jj_{\nu n}\right]. \tag{15}$$

The limiting form of Ref. 3 is embodied in Equations (8), (10), (14) and (15), which were used to obtain an alternative solution for $M = 0{\cdot}8$ with $m(N) = 11(2)$. Since the real terms in both the load distribution and boundary condition are precisely those in Equations (2) and (4) to the first order in frequency, the quasi-steady quantities such as the pitching stiffness are identical. It is reassuring that the imaginary terms in the integrated loading are found to be in good agreement.

It is unnecessary to set out the method of solution in detail, as the treatment of Equation (4) for pitching oscillations is fully described in Section 5 of Ref. 2; the load distribution is written as

$$l = \theta\bar{l}_1 + \frac{\dot{\theta}\bar{c}}{U}\left\{\frac{M^2}{1-M^2}\frac{x}{\bar{c}}\bar{l}_1 - \frac{x_0}{\bar{c}}\bar{l}_1 + \frac{1-2M^2}{1-M^2}\bar{l}_2 + \frac{1}{1-M^2}\bar{l}_3\right\}, \tag{16}$$

where θ is the instantaneous angle of pitch about the axis $x = x_0$ and $\bar{l}_1$, $\bar{l}_2$, $\bar{l}_3$ are defined in Equation (65) of Ref. 2. The corresponding expression in the treatment of Equation (10) is

$$l = \theta \bar{l}_1 + \frac{\dot{\theta}\bar{c}}{U}\left\{ -\frac{x}{\bar{c}}\bar{l}_1 - \frac{x_0}{\bar{c}}\bar{l}_1 + 2\bar{l}_2 + \frac{1}{1-M^2}\bar{l}_4 \right\}, \tag{17}$$

where $\bar{l}_4$ is formally equivalent to $\bar{l}_3$, the influence functions ii and jj being replaced by

$$[(\tfrac{1}{4}-X)i - \tfrac{1}{16}j + ii] \text{ and } [-3i + (\tfrac{3}{4}-X)j + 3jj]$$

in accord with Equations (14) and (15) respectively.

The lift and pitching-moment coefficients are readily evaluated from the integrals

$$\left.\begin{aligned} C_L &= \int_0^1 \int_0^\pi [lc/2\bar{c}] \sin\phi \, d\phi \, d\eta \\ C_m &= \int_0^1 \int_0^\pi [lc(x_0-x)/2\bar{c}^2] \sin\phi \, d\phi \, d\eta \end{aligned}\right\}. \tag{18}$$

The pitching derivatives are then defined by

$$\left.\begin{aligned} C_L &= -2[\theta z_\theta + (\dot{\theta}\bar{c}/U)z_{\dot{\theta}}] \\ C_m &= 2[\theta m_\theta + (\dot{\theta}\bar{c}/U)m_{\dot{\theta}}] \end{aligned}\right\} \tag{19}$$

and are finally expressed, as in Table 1, by formulae

$$\left.\begin{aligned} -z_\theta &= A - Bh \\ -z_{\dot{\theta}} &= C - Dh \\ -m_\theta &= E + Fh + Bh^2 \\ -m_{\dot{\theta}} &= G + Hh + Dh^2 \end{aligned}\right\}, \tag{20}$$

where $h = x_0/\bar{c}$ and for low frequency $A = D = -F$, $B = 0$ and $C + E + H = 0$.

To cover the range of experiments on the M-wing, a bending mode must also be considered. The equation of the surface of a wing bending rigidly about its centre-line is

$$z = \phi_0 |y| e^{i\omega t},$$

so that the boundary condition is

$$\begin{aligned} w &= i\omega s \phi_0 |\eta| e^{i\omega t} \\ &= \dot{\phi} s |\eta|, \end{aligned} \tag{21}$$

where $\dot{\phi}$ is the instantaneous rate of change of angle of bend.

Whenever there are spanwise discontinuities in $w(\eta)$ or its derivatives, it is advisable to use an equivalent smooth distribution. Such a procedure has been discussed and formulated for part-span control surfaces in Ref. 5. The required values $w_\nu = w(\eta_\nu)$ are represented by equivalent quantities

$$-w_{e\nu} = 2U\left[b_{\nu\nu}\gamma_{\nu 0} - \sum_{-\frac{1}{2}(m-1)}^{\frac{1}{2}(m-1)\prime} b_{\nu n}\gamma_{n0} \right], \tag{22}$$

where $\gamma_{n0} = \gamma_0(\eta_n)$ is the exact solution of Equation (21) by low-aspect-ratio theory[6] (De Young), namely,

$$\gamma_0 = -\frac{\dot{\phi}s}{\pi}\left\{\sin\psi - \cos^2\psi \log_e\left|\frac{\cos\psi}{1+\sin\psi}\right|\right\}, \tag{23}$$

where $\eta = \cos\psi$. Comparative values of $|\eta_\nu|$ and $w_{e\nu}/\dot{\phi}s$ are given below:

$\lvert\eta_\nu\rvert$	$m = 11$		$m = 23$	
	ν	$w_{e\nu}/\dot{\phi}s$	ν	$w_{e\nu}/\dot{\phi}s$
0	0	0·0371	0	0·0184
0·1305			1	0·1323
0·2588	1	0·2623	2	0·2582
0·3827			3	0·3833
0·5000	2	0·4987	4	0·4997
0·6088			5	0·6090
0·7071	3	0·7084	6	0·7070
0·7934			7	0·7935
0·8660	4	0·8653	8	0·8660
0·9239			9	0·9241
0·9659	5	0·9667	10	0·9658
0·9914			11	0·9916

Calculations have been made with $m(N) = 11(2)$ and $23(2)$ for both $M = 0$ and $M = 0{\cdot}8$. The alternative conditions $w_\nu = w_{c\nu}$ and $w_\nu = \dot{\phi}s\,|\eta_\nu|$ are shown to give results in very close agreement.

Since w is $0(\omega)$, the low-frequency solution is quasi-steady and with $N = 2$ Equation (4) or (10) reduces to

$$-w/U = b_{\nu\nu}[\bar{i}_{\nu\nu}\bar{\gamma}_\nu + \bar{j}_{\nu\nu}\bar{\mu}_\nu] - \sum_{-\frac{1}{2}(m-1)}^{\frac{1}{2}(m-1)}{}' b_{\nu n}[i_{\nu n}\bar{\gamma}_n + j_{\nu n}\bar{\mu}_n] + O(\omega^2)\,. \tag{24}$$

With spanwise symmetry the values of $\bar{\gamma}_n$ and $\bar{\mu}_n$ from the $(m+1)$ simultaneous equations lead to the load distribution in Equation (2);

$$l = (\dot{\phi}s/U)\bar{l}\,,$$

where $\bar{l}$ is real and corresponds to the steady condition $w/U = |\eta|$. Hence the lift is given by Equation (18) and the bending-moment coefficient is

$$C_b = \frac{B}{\rho U^2 S s} = \int_0^1\int_0^\pi (lc/4\bar{c})\eta\sin\phi\,d\phi\,d\eta\,. \tag{25}$$

The bending derivatives are then defined by

$$\left.\begin{aligned} C_L &= -2(\dot{\phi}s/U)z_{\dot{\phi}} \\ C_b &= (\dot{\phi}s/U)b_{\dot{\phi}} \end{aligned}\right\}. \tag{26}$$

The steady rolling derivative l_p, defined by

$$C_l = \frac{\mathscr{L}}{\rho U^2 Ss} = \left(\frac{ps}{U}\right) l_p,$$

where p is the rate of roll, has also been calculated by satisfying the antisymmetrical boundary condition $w = ps\eta$.

3. *Calculations for Finite Frequency Parameter.* In order to investigate the behaviour of the wing when the frequency parameter is not small, some calculations have been carried out by the method of Ref. 3, which is essentially an extension of Ref. 2 to finite frequency. The loading is assumed to be that in Equation (8).

The values of the frequency parameter were taken to be $\bar{\nu} = \omega\bar{c}/U = 0{\cdot}3$ and $0{\cdot}6$, and the Mach number $M = 0{\cdot}8$ throughout. The collocation points were chosen to be the same as those for the low-frequency calculation with $m(N) = 11(2)$. The influence functions

$$\left.\begin{aligned} I &= i_1 + i_2 + i_3 + i_4 \\ \text{and} \qquad J &= j_1 + j_2 + j_3 + j_4 \end{aligned}\right\} \tag{27}$$

had then to be calculated from Equations (47) to (59) of Ref. 3 for the appropriate values of X and Y in Equation (6). The functions i_3, i_4, j_3 and j_4 were calculated mechanically on the DEUCE by the Mathematics Division, N.P.L., but i_1 and i_2 were evaluated on desk machines and both j_1 and j_2 are identically zero. No difficulty was encountered in any of these computations. For each collocation point the upwash w prescribed by the motion of the wing is inserted in Equation (10), where the quantities $\bar{I}_{\nu\nu}$ and $\bar{J}_{\nu\nu}$ are corrected for the logarithmic singularity by Equations (62) and (63) of Ref. 3. The resulting set of 12 complex simultaneous equations were solved mechanically to give the required values of γ and μ at the six spanwise locations $\eta_n = \sin[n\pi/(m+1)]$ with $n = 0, 1, \ldots \frac{1}{2}(m-1)$.

Since the evaluation of the influence functions for the low-frequency case is much quicker than for a finite frequency, some calculations were made in which the elements in the matrix of the simultaneous equations were replaced by the corresponding values calculated by low-frequency theory. Thus in accord with Equations (14) and (15)

$$\left.\begin{aligned} I_{\nu n} &= i_{\nu n} - \frac{i\bar{\nu}}{1-M^2}\frac{c_n}{\bar{c}}\left[\left(\tfrac{1}{4} - X_{\nu n}\right)i_{\nu n} - \tfrac{1}{16}j_{\nu n} + ii_{\nu n}\right] \\ J_{\nu n} &= j_{\nu n} - \frac{i\bar{\nu}}{1-M^2}\frac{c_n}{\bar{c}}\left[-3i_{\nu n} + \left(\tfrac{3}{4} - X_{\nu n}\right)j_{\nu n} + 3ji_{\nu n}\right] \end{aligned}\right\}, \tag{28}$$

where $\bar{\nu}$ was given the appropriate numerical value. The calculations were otherwise identical to those described above. Unfortunately the results of this 'hybrid' method in Table 1 differ widely from those using the exact influence functions, although the direction of the trend with frequency is correctly predicted.

The lift is given by the formula

$$L = \tfrac{1}{2}\rho U^2 SA \int_{-1}^{1} \exp\left\{-\frac{i\omega(x_l + \frac{1}{2}c)}{U}\right\}\left\{\gamma(J_0 + iJ_1) + 4\mu(-J_2 + iJ_1)\right\} d\eta\,, \tag{29}$$

and the nose-up pitching moment about the axis $x = 0$ by

$$\mathscr{M}_0 = \tfrac{1}{2}\rho U^2 S\bar{c}A \int_{-1}^{1} \exp\left\{-\frac{i\omega(x_l+\frac{1}{2}c)}{U}\right\}\left\{\frac{x_l}{\bar{c}}\gamma(J_0+iJ_1)\right.$$
$$+\frac{4x_l}{\bar{c}}\mu(-J_2+iJ_1)+\frac{c\gamma}{4\bar{c}}(J_0+J_2)$$
$$\left.+\frac{c\mu}{\bar{c}}(-J_0-J_2+iJ_1+iJ_3)\right\}d\eta\,, \tag{30}$$

where $J_n \equiv J_n(\omega c/2U)$ is the Bessel function of order $n(=0, 1, 2, 3)$, of which tables are available in Ref. 7. Thus the lift and moment $\mathscr{M} = \mathscr{M}_0 + x_0 L$ are easily evaluated, and hence the pitching derivatives as defined by Equations (19). In terms of the frequency parameter

$$\left.\begin{aligned} L &= -\rho U^2 S[z_\theta + i\bar{\nu}z_{\dot{\theta}}] \\ \mathscr{M} &= \rho U^2 S\bar{c}[m_\theta + i\bar{\nu}m_{\dot{\theta}}] \end{aligned}\right\}. \tag{31}$$

The equivalent boundary condition (22) was used in obtaining the solution for the rigid bending mode of oscillation. The bending moment is given by the lift integral (29) with a factor $|y| = s|\eta|$ in the integrand; hence

$$B = \rho U^2 Ss\left[b_\phi + \frac{i\omega s}{U}b_{\dot{\phi}}\right]$$
$$= \rho U^2 Ss[b_\phi + \tfrac{1}{2}i\bar{\nu}Ab_{\dot{\phi}}]\,. \tag{32}$$

The corresponding lift may be written in the form

$$L = -\rho U^2 S(z_{\dot{\phi}} + \tfrac{1}{2}i\bar{\nu}Az_{\dot{\phi}}). \tag{33}$$

4. *Results and Discussion.* The results are contained in Tables 1 to 3 and Figs. 2 to 6. Table 1 lists the pitching derivatives as linear or quadratic functions of axis position h; they are given numerically in Table 2 for the equidistant axes $h = 0{\cdot}0650$, $0{\cdot}4644$ and $0{\cdot}8638$, for which provision is made in the experiments. Table 3 contains calculated derivatives for the symmetrical rigid-bending and antisymmetrical rolling modes.

The steady aerodynamic characteristics of the M-wing, as calculated by lifting-surface theory, are given in the following table.

$m(N)$	M	$\partial C_L/\partial\alpha$	$h_{a.c.}$	$\bar{\eta}$	C_D/C_L^2
11(2)	0	2·981	−0·4188	0·3984	0·0750
23(2)	0	2·854	−0·3834	0·3956	0·0754
11(2)	0·8	3·301	−0·4189	0·3914	0·0765
11(3)	0·8	3·391	−0·4264	0·3923	0·0762
23(2)	0·8	3·182	−0·3693	0·3943	0·0769

To summarize, the lift slope increases by 11 per cent from about 2·94 at $M = 0$ to 3·27 at $M = 0{\cdot}8$, the aerodynamic centre moves from about $0{\cdot}39\bar{c}$ to $0{\cdot}38\bar{c}$ forward of the root leading edge, while the spanwise centre of pressure stays well inboard at $\bar{\eta} = 0{\cdot}395$ and the lift-dependent drag

coefficient $0{\cdot}076C_L^2$ is 20 per cent greater than its optimum value $C_L^2/(\pi A) = 0{\cdot}063C_L^2$. The table also shows that the choice of the number of spanwise collocation sections may significantly affect the lift slope and aerodynamic centre. The increase from $m = 11$ to $m = 23$ reduces $\partial C_L/\partial\alpha$ by 4 per cent and shifts the position $h_{a.c.}$ rearward by about $0{\cdot}04\bar{c}$.

Figs. 2a and 2b show the local lift and aerodynamic centre as functions of spanwise position for $M = 0$ and $M = 0{\cdot}8$: the peaks in the curves of $X_{a.c.}$ at $\eta = 0{\cdot}5$ correspond to a smooth locus of the local aerodynamic centre as it crosses the junction of the inner and outer panels. Although $cC_{LL}/\bar{c}C_L$ shows only a small variation with m and no detectable variation with N, $X_{a.c.}$ reveals a remarkable dependence on m, which is emphasized in the table below.

$m(N)$	Values of $X_{a.c.}$ for $M = 0{\cdot}8$					
	$\eta = 0$	0·2588	0·5000	0·7071	0·8660	0·9659
11(2)	0·0243	0·2735	0·4695	0·1682	0·1293	0·0806
11(3)	0·0207	0·2551	0·4785	0·1778	0·1349	0·0710
23(2)	0·0764	0·2838	0·4968	0·2621	0·2436	0·1866

Thus over the outer panel of the M-wing, the increase from $N = 2$ to $N = 3$ only brings about fairly small changes of the order 0·01 in $X_{a.c.}$, while the increase from $m = 11$ to $m = 23$ increases $X_{a.c.}$ by 0·10. A similar trend of smaller order 0·02 has been found for arrowhead and delta wings (Ref. 8, Table XVII), though it is negligible for rectangular wings. The phenomenon is therefore attributed to sweepback, and probably arises from inaccuracy in the spanwise integration implicit in the right-hand side of Equation (4). Even for the M-wing with a discontinuity of 110 deg in sweepback at mid-semi-span, there is every reason to suppose that this could be remedied by taking a large enough value of m. It is uncertain whether calculations with $m(N) = 35(2)$ or 23(3), involving the formation and solution of 36 simultaneous equations, would establish the value of $X_{a.c.}$ to two decimal places; for this purpose it might be necessary to undertake exceedingly laborious calculations with $m(N) = 47(3)$ or 35(4) with twice that number of equations. An interesting practical consideration is to what extent the convergence of the solution would be improved or worsened by taking values of $(m+1)$ which are not multiples of 6 so that the discontinuity no longer occurs at a collocation section, or by taking an even value of m so that the central kink is also eliminated from the boundary conditions.

In the low-frequency case, $z_{\dot{\theta}}$ and $m_{\dot{\theta}}$ are given in Figs. 3a and 3b as functions of h calculated from Table 1. Fig. 3a shows that for the range of pitching axis $z_{\dot{\theta}}$ increases with Mach number. For $M = 0{\cdot}8$, the minimum value of the pitching damping derivative $-m_{\dot{\theta}} = 0{\cdot}7$ occurs for a pitching axis $h = -0{\cdot}42$ close to the aerodynamic centre; for pitching axes aft of this $-m_{\dot{\theta}}$ shows a marked increase with M. For $M = 0$, the minimum value $-m_{\dot{\theta}} = 0{\cdot}5$ is significantly higher than that calculated for many other wings, although this seems to be less true for $M = 0{\cdot}8$ (Ref. 2, Fig. 5). Fig. 3b shows, for $M = 0{\cdot}8$, the effect of changing the number of collocation points and the form of the load distribution. The full curves correspond to the limiting form of Ref. 3 as $\bar{\nu} \to 0$, which is considered in Section 2; these lie close to the result from Ref. 2 for the same $m(N) = 11(2)$. With an extra chordwise term the curves of $z_{\dot{\theta}}$ and $m_{\dot{\theta}}$ lie between the other two for some negative

values of h but diverge along the dotted curves for $h > -0{\cdot}5$. As would be expected from the previous discussion of steady theoretical results, there are rather larger discrepancies between the two dashed curves for different values of m. It seems that for the practical range of pitching axis the uncertainties in $z_{\dot\theta}$ and $m_{\dot\theta}$ are of order $\pm 0{\cdot}05$ and $\pm 0{\cdot}10$ respectively.

Since the calculations of the effect of frequency parameter were limited to $m = 11$, the numerical values of the derivatives from Table 1 must be treated with reserve. However, Figs. 4a and 4b show the curves of z_θ, $z_{\dot\theta}$ and m_θ, $m_{\dot\theta}$ for $M = 0{\cdot}8$ as functions of h for $\bar\nu = 0$, $0{\cdot}3$ and $0{\cdot}6$. It may be concluded that frequency effect is of the same order as that of Mach number but often of opposite sign. Thus $-z_{\dot\theta}$ increases with frequency and for pitching axes aft of the aerodynamic centre $-m_{\dot\theta}$ falls by roughly 30 per cent as $\bar\nu$ changes from 0 to $0{\cdot}6$. The effect of increasing $\bar\nu$ is to shift the minimum of $-m_{\dot\theta}$ to an axis further aft and reduce its value slightly. This is similar to the behaviour of $-m_{\dot\theta}$ for a rectangular wing of aspect ratio 4 (Ref. 3) and may be characteristic of wings of fairly high aspect ratio.

The four pitching derivatives are plotted against $\bar\nu$ and M in Figs. 5a and 5b for pitching axes $h = 0{\cdot}065$ and $h = -0{\cdot}734$ which lie on opposite sides of the aerodynamic centre. The theoretical curves against $\bar\nu$ are from results by Ref. 3 for $M = 0{\cdot}8$, the 'hybrid' method (Section 3) with $m(N) = 11(2)$ being included for the axis $h = 0{\cdot}065$. They have been drawn on the assumption that each derivative is of the form $(P + Q\bar\nu^2 + R\bar\nu^2 \log \bar\nu)$, except for the 'hybrid' case when the form $(P + Q\bar\nu^2 + R\bar\nu^4)$ was taken since no terms in $\bar\nu^2 \log \bar\nu$ can then appear. In each case the constants P, Q and R have been determined from the known values of the derivative for $\bar\nu = 0$, $0{\cdot}3$ and $0{\cdot}6$. As mentioned in Section 3, the results of the 'hybrid' method, in which terms of order $\bar\nu^2$ in the influence functions are ignored, differ widely from those derived from the exact influence functions of Ref. 3. The 'hybrid' method, though of no practical use, does predict correctly the trend of each derivative with frequency. The curves against $\bar\nu$ in Fig. 5b illustrate how, for both m_θ and $m_{\dot\theta}$, the effect of frequency has opposite signs for the two axis positions.

The curves against M correspond to the low-frequency theory of Ref. 2 and include the same two values of h for both $m = 11$ and $m = 23$. Since the derivatives are only known for $M = 0$ and $M = 0{\cdot}8$, special care has been taken in preparing the curves. It is explained in Ref. 2 that all the derivatives are fully expressed by the seven coefficients

$$(I_L)_1,\ (I_L)_2,\ (I_L)_3,\ I_L^* = -(I_m)_1,\ (I_m)_2,\ (I_m)_3 \text{ and } I_m^*.$$

For example, from Equation (79) of Ref. 2,

$$m_{\dot\theta} = \left\{\frac{1-\beta^2}{2\beta^3} I_m^* + \frac{2\beta^2-1}{2\beta^3}(I_m)_2 + \frac{1}{2\beta^3}(I_m)_3\right\} + h\left\{-\frac{1}{2\beta^3}(I_m)_1 + \frac{2\beta^2-1}{2\beta^3}(I_L)_2 + \frac{1}{2\beta^3}(I_L)_3\right\} - h^2 \cdot \frac{1}{2\beta}(I_L)_1, \qquad (34)$$

where $\beta = \sqrt{(1-M^2)}$. For each of the seven coefficients the formula

$$f(M) = \tfrac{1}{2}(5\beta^2 - 3\beta) f(0) + \tfrac{2}{6}\tfrac{5}{}(\beta - \beta^2) f(0{\cdot}8) \qquad (35)$$

has been used to estimate its value for any required subsonic Mach number before substitution into an expression such as Equation (34) for $m_{\dot\theta}$. This implies that

$$m_\theta(M) = \tfrac{1}{2}(5\beta - 3) m_\theta(0) + \tfrac{5}{2}(1-\beta) m_\theta(0{\cdot}8) \qquad (36)$$

and that there is an identical formula for z_θ. Although the separate curves for $m = 11$ and $m = 23$ cast doubt on numerical accuracy, there is reason to suppose that the variation of each derivative with Mach number is approximately correct. It is noteworthy that in practically every case the influences of compressibility and finite frequency are of equal order of magnitude and of opposite sign; for pitching axes close to the aerodynamic centre, neither frequency nor Mach number has much effect on the stiffness and damping derivatives.

With regard to numerical accuracy, it is concluded that z_θ, $z_{\dot\theta}$ and m_θ are liable to errors of the order $\pm 0{\cdot}05$, but that $m_{\dot\theta}$ is uncertain within about $\pm 0{\cdot}10$. However, it is possible to estimate values that may be well within these limits. For $M = 0{\cdot}8$ there are three solutions by Multhopp's theory for low frequencies, namely, $m(N) = 11(2)$, $11(3)$ and $23(2)$; the best available procedure is to apply the linear combination $\{11(3) - 11(2)\} + \{23(2) - 11(2)\}$ as a correction to the solutions by Ref. 3 for $\bar\nu = 0$, $0{\cdot}3$ and $0{\cdot}6$. When the appropriate values from Table 1 are used in this way, the recommended derivatives are obtained in the notation of formulae (20) as follows:—

$$\left.\begin{aligned} -z_\theta &= A - Bh, & -m_\theta &= E + Fh + Bh^2 \\ -z_{\dot\theta} &= C - Dh, & -m_{\dot\theta} &= G + Hh + Dh^2 \end{aligned}\right\}, \tag{37}$$

where

$\bar\nu$	A	B	C	D	E	F	G	H
0	1·64	0	−0·79	1·64	−0·62	−1·64	1·08	1·41
0·3	1·51	0·02	−0·41	1·50	−0·58	−1·47	0·91	0·97
0·6	1·36	−0·01	−0·09	1·34	−0·56	−1·26	0·75	0·56

The derivatives calculated for the rigid bending mode are summarized in Table 3 in the notation of Equations (32) and (33). The values of $z_{\dot\phi}$ and $b_{\dot\phi}$ obtained from the alternative forms of the boundary condition in Equations (21) and (22) are seen to differ only by small quantities which, especially for $b_{\dot\phi}$, are within the accuracy indicated by the calculations for different values of m. The in-phase derivatives z_ϕ and b_ϕ are small but erratic functions of $\bar\nu$. In the lower diagram of Fig. 6 the in-phase part of the local lift $(cC_{LL}/\bar c)$ is plotted against η; it can be seen that the variation of z_ϕ and b_ϕ with $\bar\nu$, particularly the negative value of $-b_\phi$ for $\bar\nu = 0{\cdot}6$, is due to a region near mid-semi-span in which the local lift increases slightly for small values of $\bar\nu$ and then becomes negative. Since $m = 11$ in these calculations, the curves in Fig. 6 must be regarded as approximate only and the sign of the stiffness derivative $-b_\phi$ is uncertain. The out-of-phase derivatives $z_{\dot\phi}$ and $b_{\dot\phi}$ both decrease as $\bar\nu$ increases, but $-b_{\dot\phi}$ remains positive and has only fallen by 16 per cent when $\bar\nu = 0{\cdot}6$, so that the bending oscillation shows no likelihood of becoming undamped. The right hand column of Table 3 gives the steady rolling derivative $-l_p$, which is always less than $-b_{\dot\phi}$. The upper diagram of Fig. 6 gives the out-of-phase part of $(cC_{LL}/\bar c)$ as a function of η for $\bar\nu = 0$, $0{\cdot}3$ and $0{\cdot}6$ and also for steady rolling. The curve for steady rolling lies below that for the symmetrical bending mode at $\bar\nu = 0$ and by antisymmetry must pass through the origin. From the values quoted in Table 3, it appears that a factor $0{\cdot}89$ should be applied to a measured value of $b_{\dot\phi}$ on the half-M-wing to obtain the corresponding antisymmetrical rolling damping coefficient.

5. *Comparison with Experiment.* The derivatives z_θ, $z_{\dot\theta}$, m_θ and $m_{\dot\theta}$ have been measured on a half-wing model of span 11 in. mounted on a side wall of the N.P.L. 25 in. by 20 in. Wind Tunnel. Streamwise slotted liners were fitted to the roof and floor of the tunnel, so that the height of the working section was reduced to 21 in. The slots were of width 0·18 in. with centres 1·98 in. apart. The experiments[9] (Bratt and Wight) included the three pitching axes of Table 2, but the lift derivatives z_θ and $z_{\dot\theta}$ were only measured for the middle axis $h = 0{\cdot}464$. The tests for this axis have been repeated subsequently with slots sealed to give a closed tunnel.

The experimental values with slotted walls at $M = 0{\cdot}8$, indicated by circles in Figs. 5b, 7a and 7b, correspond to a frequency parameter $\bar\nu = 0{\cdot}055$ and should therefore lie close to the theoretical full-line curves for low-frequency oscillations. The theoretical results in Figs. 7a and 7b are taken from the formulae (37) which are probably the least inaccurate. In fact the agreement for z_θ and m_θ is good and that for $z_{\dot\theta}$ is fairly good; the values of $m_{\dot\theta}$ show considerable discrepancies, though the trend with varying pitching axis is in accord with theory. Fig. 5b also shows the experimental variation with Mach number of the pitching-moment derivatives about the axis $h = 0{\cdot}065$. Throughout the range $0{\cdot}6 \leqslant M \leqslant 1{\cdot}0$ m_θ agrees well with the theoretical curves, while the trend of $m_{\dot\theta}$ is consistent.

The experimental values with slots sealed are also included in Figs. 7a and 7b. Since $\bar\nu$ is small, the measured values $z_\theta = -1{\cdot}81$ and $m_\theta = 1{\cdot}40$, denoted by squares, can be corrected for wall interference by the method of Ref. 10 which applies to steady flow in a closed rectangular tunnel. The free-stream derivatives for $M = 0{\cdot}8$ on this basis are

$$\left.\begin{aligned}(z_\theta)_{f.s.} &= \frac{z_\theta}{1 - 0{\cdot}032 z_\theta} = -1{\cdot}71 \\ (m_\theta)_{f.s.} &= \frac{m_\theta - 0{\cdot}011 z_\theta}{1 - 0{\cdot}032 z_\theta} = 1{\cdot}34\end{aligned}\right\}, \tag{38}$$

which are plotted as crosses and are seen to be in good agreement with low-frequency theory. No corrections have been applied to $z_{\dot\theta}$ and $m_{\dot\theta}$.

The large changes in the damping derivatives caused by sealing the slots indicate the possibility of large wall interference. There are at present no means of estimating possible slotted-wall interference effects. It might be expected that the corrections with slotted walls would resemble those for an open tunnel and be of opposite sign to those for a closed tunnel, so that the theory can be regarded as satisfactory.

6. *Conclusions.* (*a*) The theoretical aerodynamic centre of the M-wing lies at about 0·2 root chords forward of the root leading edge and shows a very small rearward movement with increasing Mach number.

(*b*) The limiting theory of Ref. 3 has been derived by letting finite frequency tend to zero. Although there are formal differences in load distribution between this and Multhopp's low-frequency theory, the derivatives calculated by the two methods agree very closely.

(*c*) As compared with conventional delta or arrowhead plan-forms, the M-wing has a high minimum pitching damping at low speeds, which occurs for a pitching axis close to the aerodynamic centre. For axes farther aft, a change in frequency parameter $\bar\nu$ from 0 to 0·6 reduces the derivative $-m_{\dot\theta}$ by roughly 30 per cent.

(*d*) Of the derivatives calculated the pitching damping is probably the least accurate. There are likely errors of the order $\pm 0{\cdot}05$ on z_θ, $z_{\dot\theta}$ and m_θ and $\pm 0{\cdot}10$ on $m_{\dot\theta}$, as given in Table 1. The formulae for $M = 0{\cdot}8$ recommended in Equation (37) are thought to be well within these limits of accuracy.

(*e*) The combination of sharp kinks at the root and mid-semi-span in both leading and trailing edges puts the theories to a severe test. Exceedingly laborious solutions with $m(N) = 35(2), 47(3)$ or higher values would be needed to establish the theoretical derivatives to two decimal places.

(*f*) The damping of the symmetrical rigid-bending mode is large and positive, while the stiffness is so small as to be of uncertain sign. A change in frequency parameter from zero to $0{\cdot}6$ reduces the derivative $-b_{\dot\phi}$ by approximately 16 per cent.

(*g*) The calculations show that a correction factor of about $0{\cdot}89$ is necessary to convert the rigid-bending damping of the half-wing model to the antisymmetrical rolling damping of the complete M-wing.

(*h*) The calculated values of z_θ and m_θ compare well with experimental results. The experimental values of $z_{\dot\theta}$ and $m_{\dot\theta}$ may be subject to considerable tunnel interference; if it can be assumed that the true experimental values lie somewhere between those measured in the slotted and closed tunnels, then the theory shows fair agreement.

7. *Acknowledgements.* The lengthy calculations were made possible by the co-operation of the DEUCE Section of the Mathematics Division, N.P.L. The authors also wish to record the assistance of Mrs. S. M. Lucas, who carried out all the desk calculations for low frequency and helped to prepare the figures, and of Miss B. Burnham, who accomplished some laborious computations associated with high frequency.

LIST OF SYMBOLS

A	Aspect ratio $= 2s/\bar{c}$
b_ϕ, $b_{\dot{\phi}}$	Stiffness and damping of bending motion in equation (32)
$b_{\nu\nu}$, $b_{\nu n}$	Spanwise integration factors in equation (24) of Ref. 2
B	Bending moment $= \rho U^2 S s C_b$
c	Local chord
$\bar{c}$	Geometric mean chord
C_b	Bending-moment coefficient
C_l	Rolling-moment coefficient
C_m	Pitching-moment coefficient
C_D	Lift-dependent drag coefficient
C_L	Lift-coefficient $= \int_0^1 (cC_{LL}/\bar{c})d\eta$
C_{LL}	Local lift coefficient $= \frac{1}{c}\int_{x_l}^{x_t} l\,dx$
D	Lift-dependent drag $= \frac{1}{2}\rho U^2 S C_D$
h	Position of pitching axis $= x_0/\bar{c}$
$h_{a.c.}$	Value of h at aerodynamic centre
i	$\sqrt{(-1)}$
i, ii, j, jj	Influence functions occurring in equations (44) and (46) of Ref. 2
$\bar{i}_{\nu\nu}$, etc.	Influence functions in final equations of Appendix II of Ref. 2
$I_{\nu n}$, $\bar{I}_{\nu\nu}$ $J_{\nu n}$, $\bar{J}_{\nu\nu}$	Influence functions occurring in Ref. 3
J_0, J_1, . . .	Bessel functions (Ref. 7)
k, kk	Extra influence functions in equation (5)
l	Wing loading = pressure difference/$\frac{1}{2}\rho U^2$
l_p	Direct steady rolling derivative (end of Section 2)
L	Lift $= \frac{1}{2}\rho U^2 S C_L$
$\mathscr{L}$	Rolling moment $= \rho U^2 S s C_l$

m	Number of spanwise collocation points
m_θ, $m_{\dot\theta}$	Stiffness and damping of pitching motion in equations (19) and (31)
M	Free-stream Mach number
$\mathscr{M}$	Pitching moment $= \frac{1}{2}\rho U^2 S\bar{c} C_m$
$\mathscr{M}_h$	Pitching moment about $x = h\bar{c}$
N	Number of chordwise collocation points
p	Angular rolling velocity
s	Semi-span of wing
S	Area of wing
t	Time
U	Free-stream velocity
w	Upward component of velocity
w_{ev}	w modified for boundary condition in equation (22)
x	Streamwise co-ordinate (Fig. 1)
x_l, x_t	Values of x at leading, trailing edge
x_0	Value of x along pitching axis
$X_{a.c.}$	Local aerodynamic centre
X, X_{vn}	Co-ordinate for influence functions in equation (6)
y	Spanwise co-ordinate (Fig. 1)
Y_{vn}	Co-ordinate for influence functions in equation (6)
z	Upward co-ordinate
z_θ, $z_{\dot\theta}$	Lift derivatives due to pitching in equations (19) and (31)
z_ϕ, $z_{\dot\phi}$	Lift derivative due to bending in equation (33)
α	Steady incidence of wing
β	Compressibility factor, $(1-M^2)^{1/2}$
γ, $\bar\gamma$	Coefficient of wing loading in equations (2) and (8)
η	Spanwise co-ordinate, y/s

η_n	$\sin [n\pi/(m+1)]$, $n = 0, \pm 1, \ldots, \pm \frac{1}{2}(m-1)$
$\bar{\eta}$	Spanwise centre of pressure
θ	Unsteady incidence of wing $= \theta_0 e^{i\omega t}$
$\dot{\theta}$	Angular pitching velocity
$\bar{\kappa}$, μ, $\bar{\mu}$	Coefficients of wing loading in equations (2) and (8)
$\bar{\nu}$	Frequency parameter $= \omega \bar{c}/U$
ρ	Free-stream density
σ_n	Imaginary quantity $= i\omega c_n/[U(1-M^2)]$
ϕ	Angular streamwise co-ordinate in equation (3)
ϕ_0	Amplitude of bending mode $z = \phi_0 \lvert y \rvert e^{i\omega t}$
$\dot{\phi}$	Angular bending velocity in equation (21)
ω	Angular frequency $= 2\pi$ (frequency)
n, ν	Suffices numerating c, x_l, γ, $\bar{\gamma}$, etc., at $\eta = \eta_n$, η_ν
νn	Double suffix numerating the influence functions
$\sum_{-\frac{1}{2}(m-1)}^{\frac{1}{2}(m-1)}{}'$	Summation with respect to n with $n = \nu$ omitted.

REFERENCES

No.	*Author(s)*	*Title, etc.*
1	H. Multhopp	Methods for calculating the lift distribution of wings (Subsonic lifting surface theory). R. & M. 2884. January, 1950.
2	H. C. Garner	Multhopp's subsonic lifting surface theory of wings in slow pitching oscillations. R. & M. 2885. July, 1952.
3	W. E. A. Acum	Theory of lifting surfaces oscillating at general frequencies in a stream of high subsonic Mach number. (With an Appendix by Miss D. E. Lehrian.) A.R.C. 17,824—O.1205—Comp.81. 30th August, 1955; and Corrigenda. 25th October, 1956.
4	K. W. Mangler and B. F. R. Spencer	Some remarks on Multhopp's subsonic lifting surface theory. R. & M. 2926. August, 1952.
5	H. C. Garner	Note on the theoretical treatment of part-span control surfaces in subsonic flow. [In preparation.]
6	J. DeYoung	Spanwise loading for wings and control surfaces of low aspect ratio. N.A.C.A. Tech. Note 2011. January, 1950.
7	G. N. Watson	A Treatise on the Theory of Bessel Functions. 2nd Edition, C.U.P., 1948.
8	H. C. Garner	Swept-wing loading. A critical comparison of four subsonic vortex sheet theories. (With a Foreword by L. W. Bryant.) C.P. 102. 1952.
9	J. B. Bratt and K. C. Wight ..	Measurements of pitching oscillation derivatives at subsonic and transonic speeds for an M-wing. A.R.C. 21,661. February, 1960.
10	H. C. Garner and W. E. A. Acum ..	Interference corrections for asymmetrically loaded wings in closed rectangular wind tunnels. R. & M. 2948. September, 1953.

TABLE 1

Summary of Calculated Pitching Derivatives

Solution	Method	$m(N)$	M	$\bar{\nu}$	A	B	C	D	E	F	G	H
1	Ref. 2	11(2)	0	0	1·4904	0	−0·0884	1·4904	−0·6242	−1·4904	0·6932	0·7126
2	Ref. 2	23(2)	0	0	1·4269	0	−0·1634	1·4269	−0·5470	−1·4269	0·5932	0·7104
3	Ref. 2	11(2)	0·8	0	1·6504	0	−0·6310	1·6504	−0·6913	−1·6504	1·1249	1·3224
4	Ref. 2	11(3)	0·8	0	1·6956	0	−0·6989	1·6956	−0·7230	−1·6956	1·2186	1·4219
5	Ref. 2	23(2)	0·8	0	1·5908	0	−0·7553	1·5908	−0·5875	−1·5908	0·9775	1·3428
6	Ref. 3	11(2)	0·8	0	1·6504	0	−0·5980	1·6504	−0·6913	−1·6504	1·1382	1·2893
7	Ref. 3	11(2)	0·8	0·3	1·5225	0·0251	−0·2199	1·5174	−0·6516	−1·4841	0·9652	0·8480
8	Ref. 3	11(2)	0·8	0·6	1·3761	−0·0116	0·1051	1·3584	−0·6302	−1·2777	0·8030	0·4399
9	Hybrid	11(2)	0·8	0·3	1·6256	0·0539	−0·5196	1·6206	−0·7060	−1·5748	1·0958	1·2013
10	Hybrid	11(2)	0·8	0·6	1·5821	0·1648	−0·3066	1·5600	−0·7651	−1·4038	1·0056	0·9751

The derivatives may be calculated from the formulae

$$-z_\theta = A - Bh, \qquad -m_\theta = E + Fh + Bh^2$$

$$-z_{\dot{\theta}} = C - Dh, \qquad -m_{\dot{\theta}} = G + Hh + Dh^2.$$

TABLE 2

Theoretical Pitching Derivatives for Particular Axes of Oscillation

		Solution from Table 1							
		1	2	3	4	5	6	7	8
Derivative	h	$M = 0$ $\bar{\nu} = 0$	$M = 0$ $\bar{\nu} = 0$	$M = 0{\cdot}8$ $\bar{\nu} = 0$	$M = 0{\cdot}8$ $\bar{\nu} = 0$	$M = 0{\cdot}8$ $\bar{\nu} = 0$	$M = 0{\cdot}8$ $\bar{\nu} = 0$	$M = 0{\cdot}8$ $\bar{\nu} = 0{\cdot}3$	$M = 0{\cdot}8$ $\bar{\nu} = 0{\cdot}6$
$-z_\theta$	0·0650	1·490	1·427	1·650	1·696	1·591	1·650	1·521	1·377
	0·4644	1·490	1·427	1·650	1·696	1·591	1·650	1·511	1·381
	0·8638	1·490	1·427	1·650	1·696	1·591	1·650	1·501	1·386
$-z_{\dot{\theta}}$	0·0650	−0·185	−0·256	−0·738	−0·809	−0·859	−0·705	−0·319	0·017
	0·4644	−0·781	−0·826	−1·398	−1·486	−1·494	−1·364	−0·925	−0·526
	0·8638	−1·376	−1·396	−2·057	−2·164	−2·130	−2·024	−1·531	−1·068
$-m_\theta$	0·0650	−0·721	−0·640	−0·799	−0·833	−0·691	−0·799	−0·748	−0·713
	0·4644	−1·316	−1·210	−1·458	−1·510	−1·326	−1·458	−1·335	−1·226
	0·8638	−1·912	−1·780	−2·117	−2·188	−1·962	−2·117	−1·915	−1·743
$-m_{\dot{\theta}}$	0·0650	0·746	0·645	1·218	1·318	1·071	1·229	1·027	0·837
	0·4644	1·346	1·231	2·095	2·245	1·944	2·093	1·686	1·300
	0·8638	2·421	2·272	3·499	3·712	3·325	3·484	2·830	2·197

TABLE 3

Summary of Calculated Bending and Rolling Derivatives

Method	$m(N)$	M	$\bar{\nu}$	$w_\nu = w_{e\nu}$ [Equation (22)]				$w_\nu = \dot{\phi}\, s\, \lvert\eta_\nu\rvert$		$-l_p$
				z_ϕ	$-b_\phi$	$z_{\dot{\phi}}$	$-b_{\dot{\phi}}$	$z_{\dot{\phi}}$	$-b_{\dot{\phi}}$	
M–G	11(2)	0	0	0	0	0·6155	0·3139	0·6055	0·3121	0·2794
M–G	23(2)	0	0	0	0	0·5869	0·2984	0·5844	0·2980	0·2670
M–G	11(2)	0·8	0	0	0	0·6750	0·3355	0·6639	0·3335	0·2926
M–G	23(2)	0·8	0	0	0	0·6569	0·3295	0·6543	0·3290	0·2906
Acum	11(2)	0·8	0·3	0·0399	0·0116	0·6168	0·3077	—	—	—
Acum	11(2)	0·8	0·6	0·0400	−0·0006	0·5378	0·2811	—	—	—

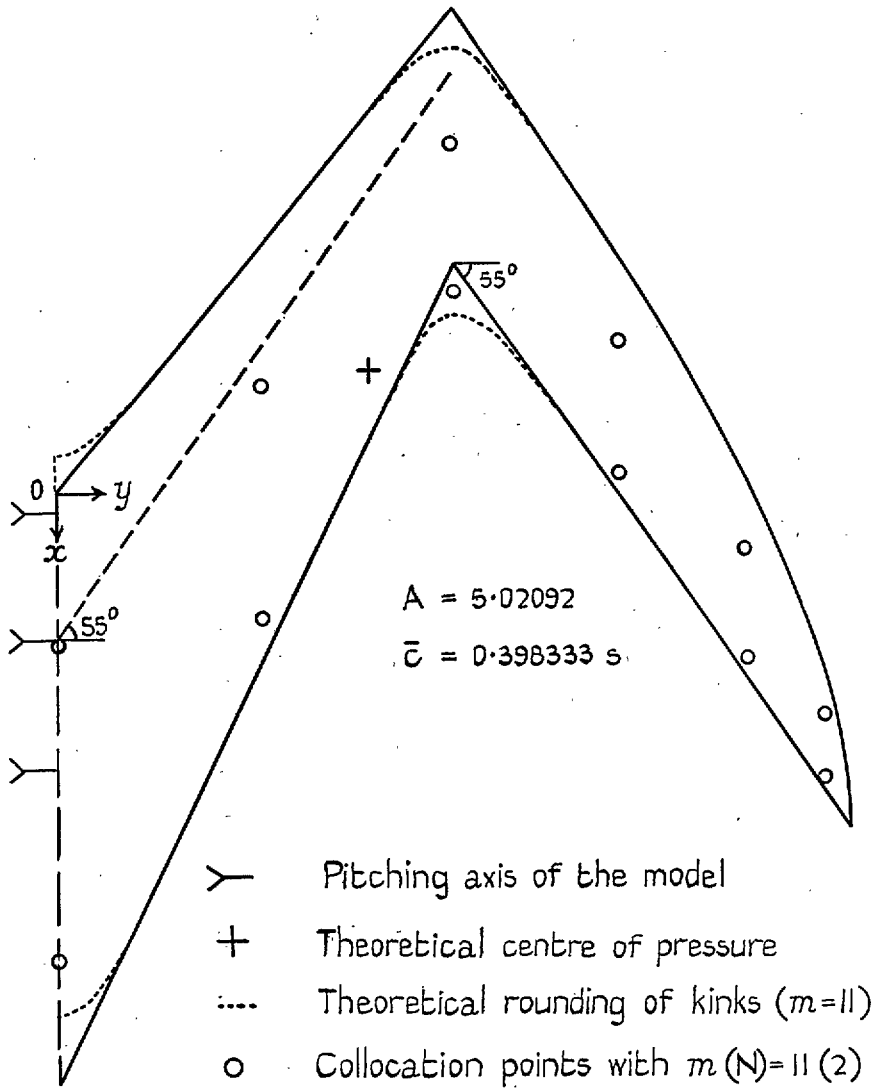

Wing chord in terms of span s of half-wing

$$c = 0{\cdot}74\,s - 0{\cdot}84\,y \qquad \text{for } 0 \leqslant y \leqslant \tfrac{1}{2}s$$
$$= 0{\cdot}64\left[\sqrt{2s(s-y)} - (s-y)\right] \qquad \text{for } \tfrac{1}{2}s \leqslant y \leqslant s$$

Equation of trailing edge

$$x = x_t = 0{\cdot}74\,s - 2{\cdot}058148\,y \qquad \text{for } 0 \leqslant y \leqslant \tfrac{1}{2}s$$
$$= -1{\cdot}003148\,s + 1{\cdot}428148\,y \qquad \text{for } \tfrac{1}{2}s \leqslant y \leqslant s$$

FIG. 1. Plan-form and details of half M-wing.

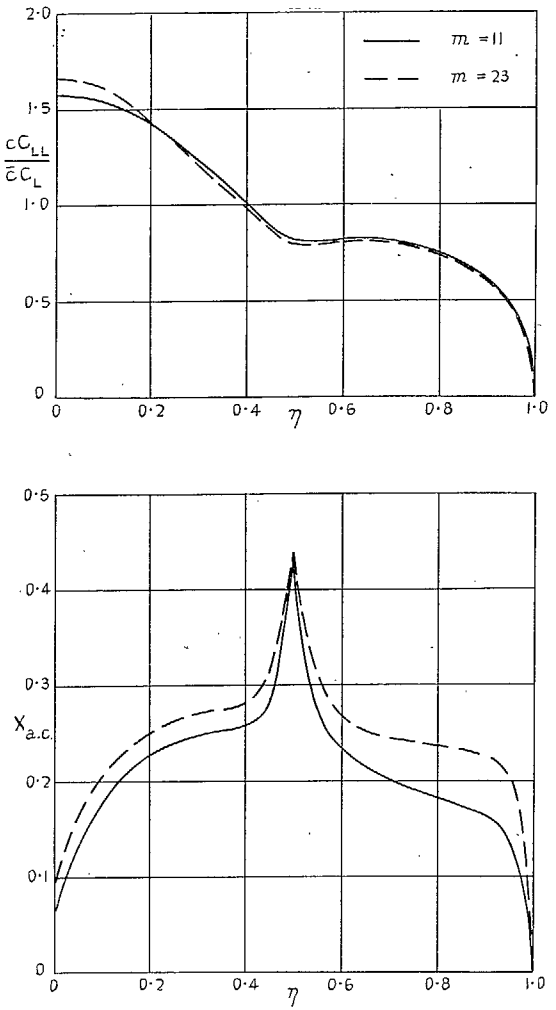

FIG. 2a. Spanwise lift distribution and local aerodynamic centre for $M = 0$.

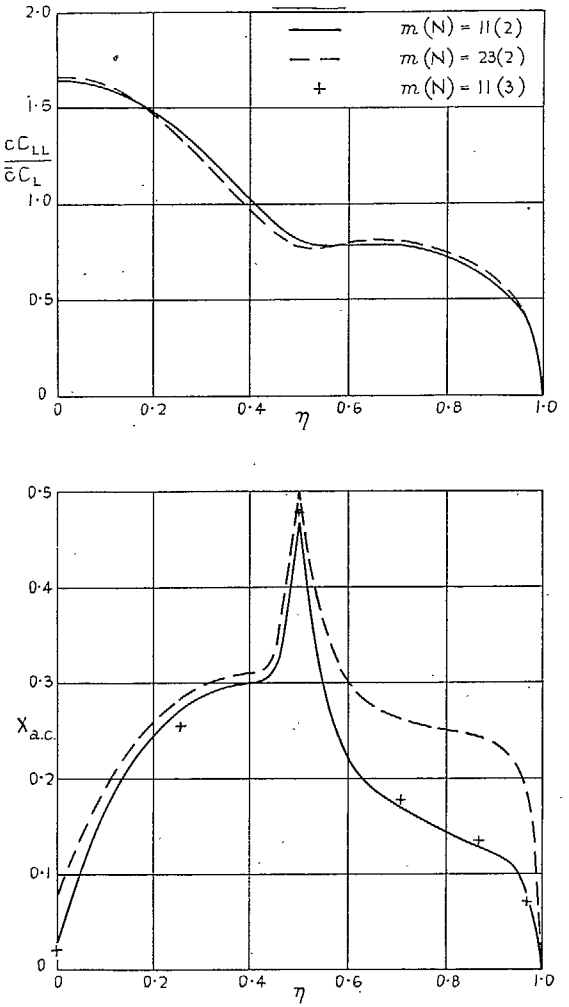

FIG. 2b. Spanwise lift distribution and local aerodynamic centre for $M = 0{\cdot}8$.

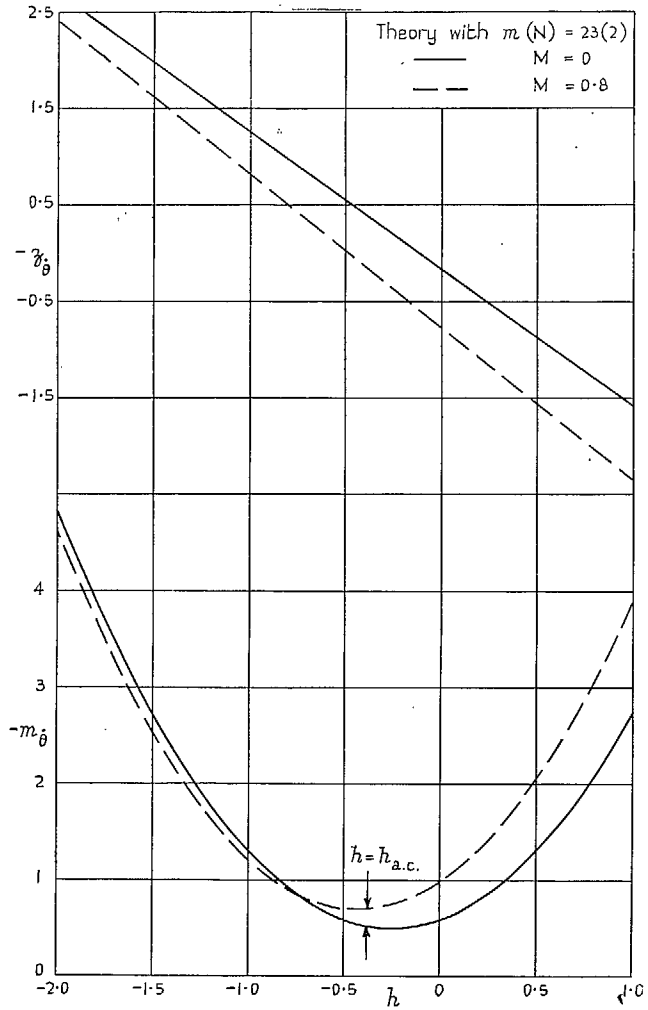

FIG. 3a. Low-frequency pitching derivatives against axis position.

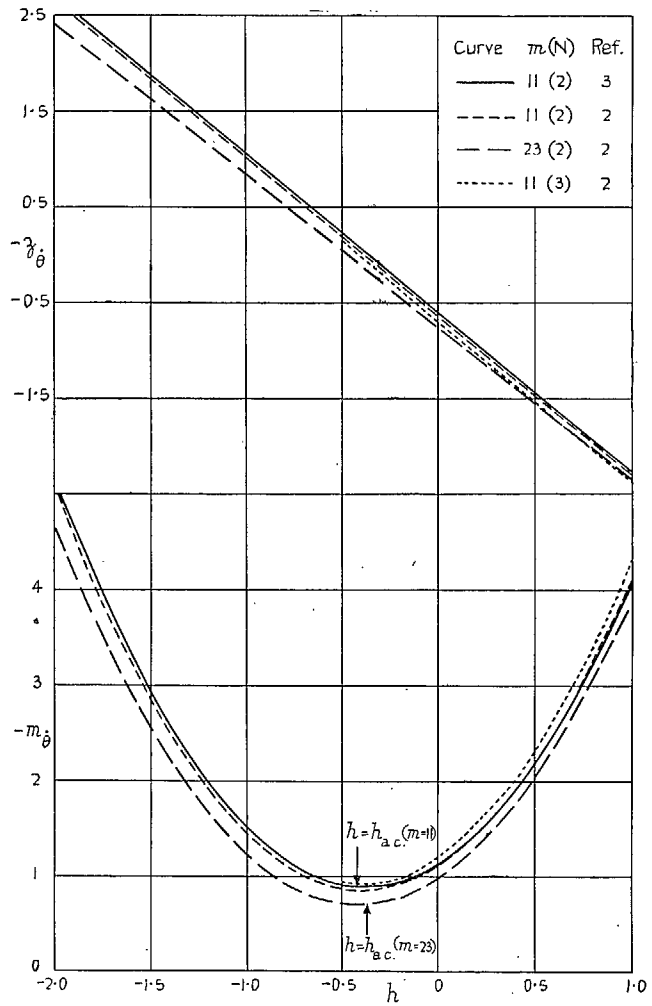

FIG. 3b. Accuracy of low-frequency pitching derivatives for $M = 0{\cdot}8$.

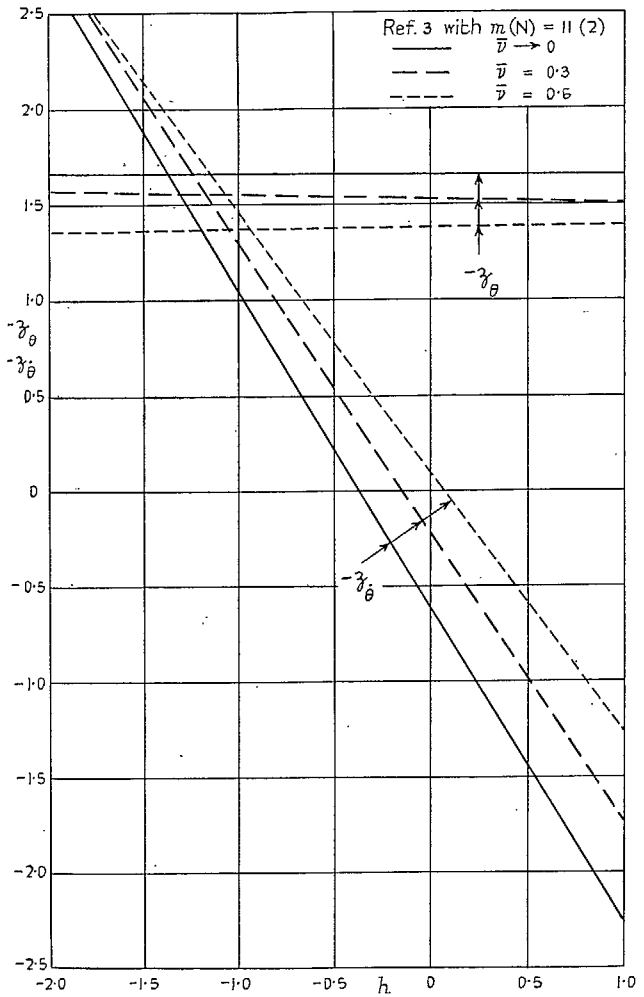

FIG. 4a. Effect of frequency on lift derivatives against pitching axis for $M = 0{\cdot}8$.

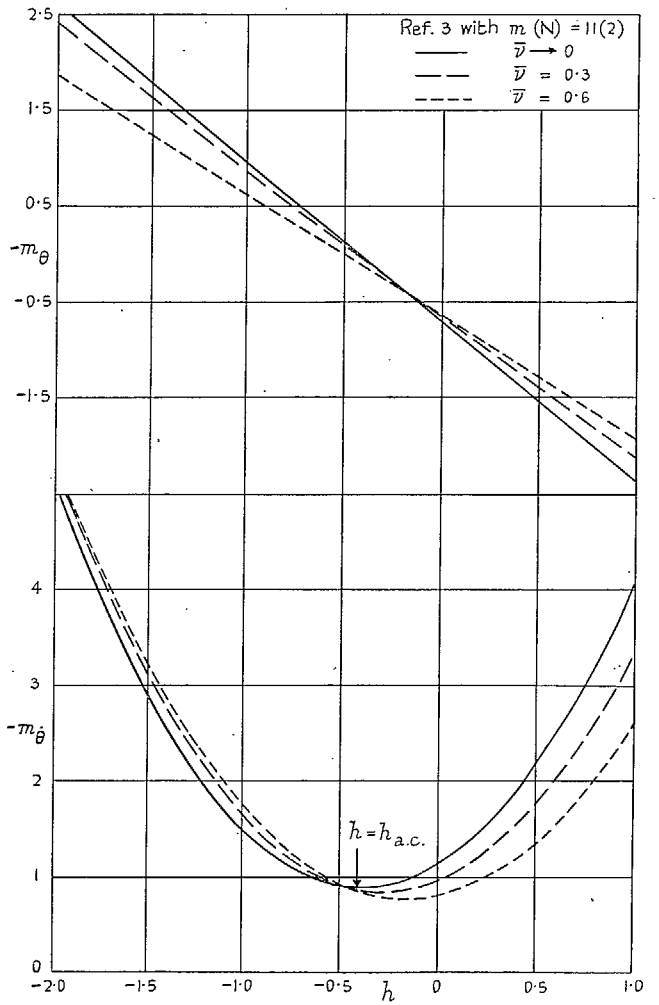

FIG. 4b. Effect of frequency on pitching stiffness and damping for $M = 0{\cdot}8$.

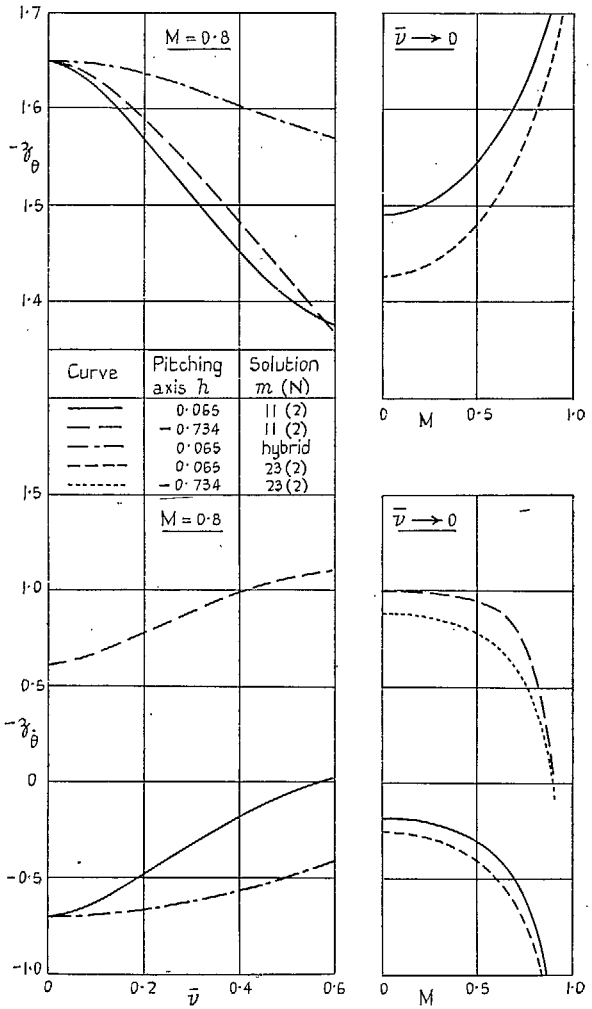

FIG. 5a. Estimated variation of lift derivatives with frequency and Mach number.

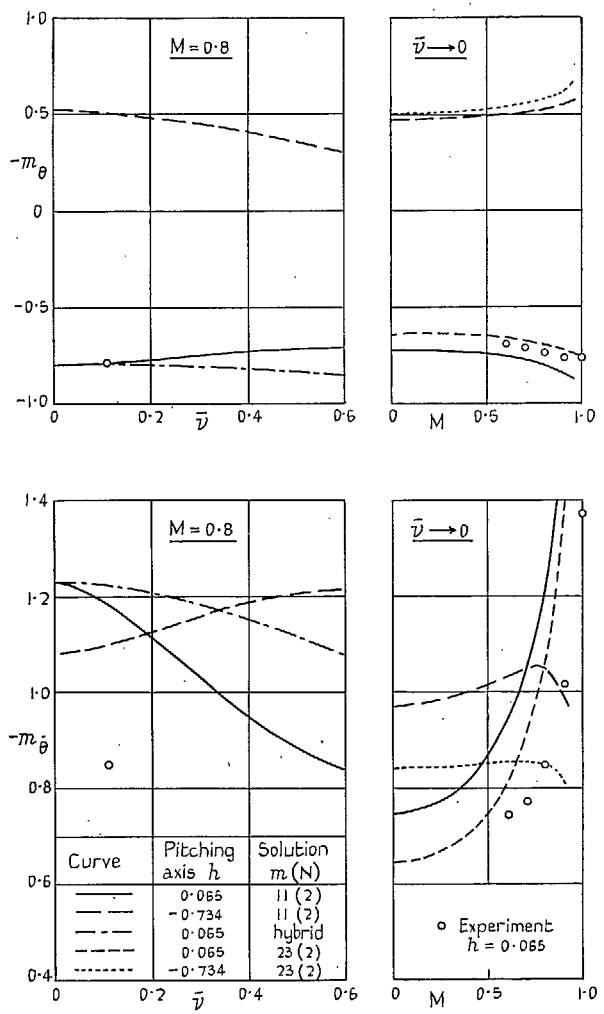

FIG. 5b. Estimated variation of pitching stiffness and damping with frequency and Mach number.

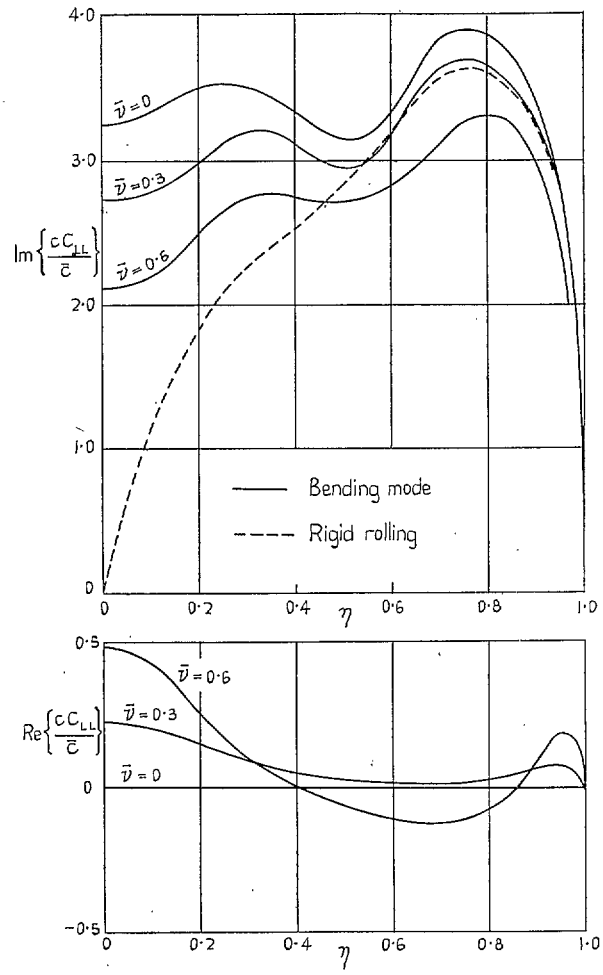

FIG. 6. Spanwise lift distribution due to bending and rolling modes.

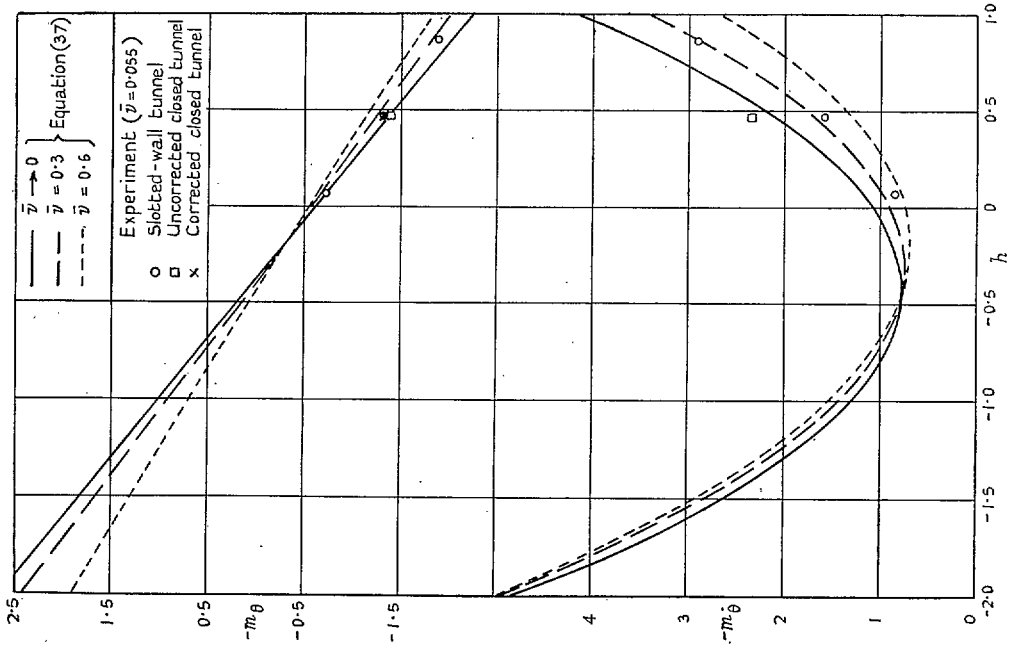

FIG. 7b. Comparison with experimental pitching stiffness and damping for $M = 0{\cdot}8$.

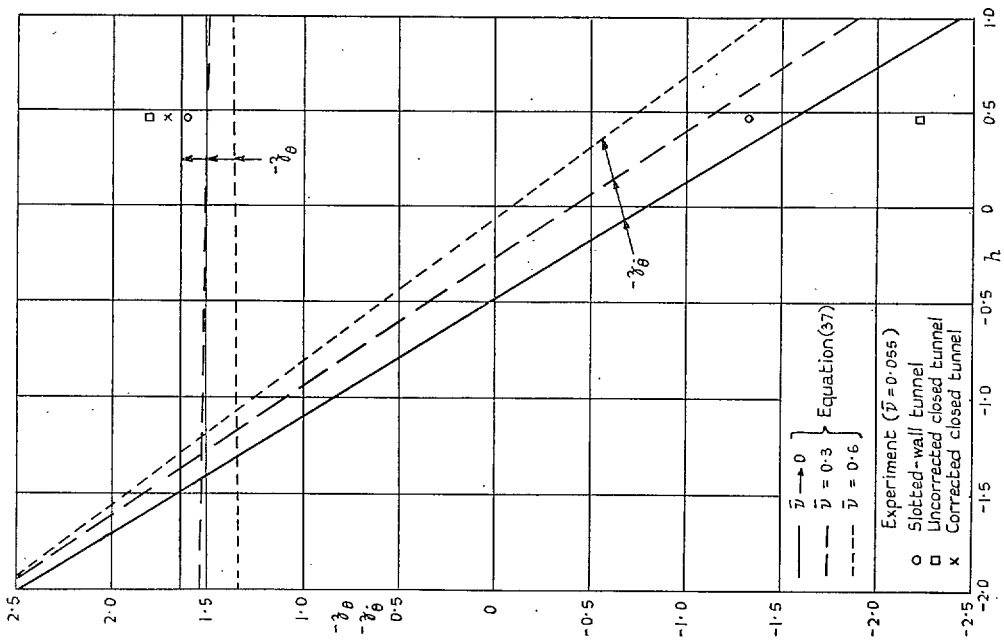

FIG. 7a. Comparison with experimental lift derivatives for $M = 0{\cdot}8$.

(82140) Wt. 66/991 K.5 9/61 Hw.

R. & M. No. 3214.
January, 1959.
H. C. Garner and W. E. A. Acum, Nat. Phys. Lab.

THEORETICAL SUBSONIC DERIVATIVES FOR AN OSCILLATING M-WING

The report describes a theoretical investigation in support of measurements being made on a half-model oscillating in pitching and rigid bending modes. Derivatives of lift and moment are tabulated and plotted as functions of pitching axis, frequency parameter and Mach number. Accuracy of calculation is discussed and some conclusions are drawn about longitudinal characteristics of the M-wing and the estimation of rolling damping from half-wing tests.

R. & M. No. 3214.
January, 1959.
H. C. Garner and W. E. A. Acum, Nat. Phys. Lab.

THEORETICAL SUBSONIC DERIVATIVES FOR AN OSCILLATING M-WING

The report describes a theoretical investigation in support of measurements being made on a half-model oscillating in pitching and rigid bending modes. Derivatives of lift and moment are tabulated and plotted as functions of pitching axis, frequency parameter and Mach number. Accuracy of calculation is discussed and some conclusions are drawn about longitudinal characteristics of the M-wing and the estimation of rolling damping from half-wing tests.

R. & M. No. 3214.
January, 1959.
H. C. Garner and W. E. A. Acum, Nat. Phys. Lab.

THEORETICAL SUBSONIC DERIVATIVES FOR AN OSCILLATING M-WING

The report describes a theoretical investigation in support of measurements being made on a half-model oscillating in pitching and rigid bending modes. Derivatives of lift and moment are tabulated and plotted as functions of pitching axis, frequency parameter and Mach number. Accuracy of calculation is discussed and some conclusions are drawn about longitudinal characteristics of the M-wing and the estimation of rolling damping from half-wing tests.

Publications of the Aeronautical Research Council

ANNUAL TECHNICAL REPORTS OF THE AERONAUTICAL RESEARCH COUNCIL (BOUND VOLUMES)

1941 Aero and Hydrodynamics, Aerofoils, Airscrews, Engines, Flutter, Stability and Control, Structures. 63*s.* (post 2*s.* 3*d.*)

1942 Vol. I. Aero and Hydrodynamics, Aerofoils, Airscrews, Engines. 75*s.* (post 2*s.* 3*d.*)
Vol. II. Noise, Parachutes, Stability and Control, Structures, Vibration, Wind Tunnels. 47*s.* 6*d.* (post 1*s.* 9*d.*)

1943 Vol. I. Aerodynamics, Aerofoils, Airscrews. 80*s.* (post 2*s.*)
Vol. II. Engines, Flutter, Materials, Parachutes, Performance, Stability and Control, Structures. 90*s.* (post 2*s.* 3*d.*)

1944 Vol. I. Aero and Hydrodynamics, Aerofoils, Aircraft, Airscrews, Controls. 84*s.* (post 2*s.* 6*d.*)
Vol. II. Flutter and Vibration, Materials, Miscellaneous, Navigation, Parachutes, Performance, Plates and Panels, Stability, Structures, Test Equipment, Wind Tunnels. 84*s.* (post 2*s.* 6*d.*)

1945 Vol. I. Aero and Hydrodynamics, Aerofoils. 130*s.* (post 3*s.*)
Vol. II. Aircraft, Airscrews, Controls. 130*s.* (post 3*s.*)
Vol. III. Flutter and Vibration, Instruments, Miscellaneous, Parachutes, Plates and Panels, Propulsion. 130*s.* (post 2*s.* 9*d.*)
Vol. IV. Stability, Structures, Wind Tunnels, Wind Tunnel Technique. 130*s.* (post 2*s.* 9*d.*)

1946 Vol. I. Accidents, Aerodynamics, Aerofoils and Hydrofoils. 168*s.* (post 3*s.* 3*d.*)
Vol. II. Airscrews, Cabin Cooling, Chemical Hazards, Controls, Flames, Flutter, Helicopters, Instruments and Instrumentation, Interference, Jets, Miscellaneous, Parachutes. 168*s.* (post 2*s.* 9*d.*)
Vol. III. Performance, Propulsion, Seaplanes, Stability, Structures, Wind Tunnels. 168*s.* (post 3*s.*)

1947 Vol. I. Aerodynamics, Aerofoils, Aircraft. 168*s.* (post 3*s.* 3*d.*)
Vol. II. Airscrews and Rotors, Controls, Flutter, Materials, Miscellaneous, Parachutes, Propulsion, Seaplanes, Stability, Structures, Take-off and Landing. 168*s.* (post 3*s.* 3*d.*)

Special Volumes

Vol. I. Aero and Hydrodynamics, Aerofoils, Controls, Flutter, Kites, Parachutes, Performance, Propulsion, Stability. 126*s.* (post 2*s.* 6*d.*)
Vol. II. Aero and Hydrodynamics, Aerofoils, Airscrews, Controls, Flutter, Materials, Miscellaneous, Parachutes, Propulsion, Stability, Structures. 147*s.* (post 2*s.* 6*d.*)
Vol. III. Aero and Hydrodynamics, Aerofoils, Airscrews, Controls, Flutter, Kites, Miscellaneous, Parachutes, Propulsion, Seaplanes, Stability, Structures, Test Equipment. 189*s.* (post 3*s.* 3*d.*)

Reviews of the Aeronautical Research Council

1939–48 3*s.* (post 5*d.*) 1949–54 5*s.* (post 5*d.*)

Index to all Reports and Memoranda published in the Annual Technical Reports

1909–1947 R. & M. 2600 6*s.* (post 2*d.*)

Indexes to the Reports and Memoranda of the Aeronautical Research Council

Between Nos. 2351–2449	R. & M. No. 2450 2*s.* (post 2*d.*)
Between Nos. 2451–2549	R. & M. No. 2550 2*s.* 6*d.* (post 2*d.*)
Between Nos. 2551–2649	R. & M. No. 2650 2*s.* 6*d.* (post 2*d.*)
Between Nos. 2651–2749	R. & M. No. 2750 2*s.* 6*d.* (post 2*d.*)
Between Nos. 2751–2849	R. & M. No. 2850 2*s.* 6*d.* (post 2*d.*)
Between Nos. 2851–2949	R. & M. No. 2950 3*s.* (post 2*d.*)
Between Nos. 2951–3049	R. & M. No. 3050 3*s.* 6*d.* (post 2*d.*)

HER MAJESTY'S STATIONERY OFFICE

from the addresses overleaf

Printed and published by
HER MAJESTY'S STATIONERY OFFICE

To be purchased from
York House, Kingsway, London W.C.2
423 Oxford Street, London W.1
13A Castle Street, Edinburgh 2
109 St. Mary Street, Cardiff
39 King Street, Manchester 2
50 Fairfax Street, Bristol 1
2 Edmund Street, Birmingham 3
80 Chichester Street, Belfast 1
or through any bookseller

Printed in England

S.O. Code No. 23-3214